Polymer 268 (2023) 125699

Contents lists available at ScienceDirect

Polymer

journal homepage: www.elsevier.com/locate/polymer

Inter and intra molecular dynamics in poly(trimethylene 2,5-furanoate) as revealed by infrared and Broadband Dielectric Spectroscopies

Oscar Gálvez [a,**], Oscar Toledano [a], Francisco Javier Hermoso [a], Amelia Linares [b], Mikel Sanz [a], Esther Rebollar [c], Aurora Nogales [b], Mari Cruz García-Gutiérrez [b], Gonzalo Santoro [b], Izabela Irska [d], Sandra Paszkiewicz [d], Anna Szymczyk [d], Tiberio A. Ezquerra [b,*]

[a] Universidad Nacional de Educación a Distancia (UNED), Depto. Física Interdisciplinar, Fac. Ciencias Av. de Esparta s/n, 28232, Las Rozas, Madrid, Spain
[b] Instituto de Estructura de la Materia, IEM-CSIC, Serrano 121, 28006, Madrid, Spain
[c] Instituto de Química Física Rocasolano, IQFR-CSIC, Serrano 119, 28006, Madrid, Spain
[d] Department of Mechanical Engineering and Mechatronics, West Pomeranian University of Technology, Al. Piastów 19, PL 70310 Szczecin, Poland

ARTICLE INFO

Keywords:
Poly(alkylene 2,5-furanoate)s
Infrared spectroscopy
Broadband dielectric spectroscopy
Barrier properties
Dielectric relaxation

ABSTRACT

Infrared spectroscopy (IR) and Broadband Dielectric Spectroscopy (BDS) experiments have been performed in poly(trimethylene 2,5-furanoate)(PTF) and poly(trimethylene terephthalate)(PTT) below their glass transition temperatures. The BDS experiments reveal a richer inter-molecular dynamic for PTT as characterized by a multimodal β relaxation in contrast with the monomodal one exhibited by PTF. The evolution with temperature of comparable IR absorption bands is very similar for PTF and PTT and shows small shifts in wavenumbers towards lower values, with exception of the band related to the stretching mode of the carbonyl group. In addition, a significant difference appears in the shape of the bands associated with the –C═O stretching. While for PTT the absorption feature is comprised of a single component, that for PTF exhibits several components suggesting the presence of hydrogen bonds. This effect may be responsible for the monomodal shape of the β relaxation of PTF since a higher degree of intramolecular coupling between the furan ring and the rest of the monomer is expected. Density Functional Theory (DFT) calculations support the experimental results revealing that as temperature increases an increment of the syn conformations of the 2,5-furandicarboxylic acid (FDCA) moiety is likely to occur in the amorphous state. The energy gain from more stable anti to less stable syn isomers can be compensated by the formation of hydrogen bonds between interchain FDCA moieties in syn conformations. This effect may cause additional hindrance to the intermolecular dynamics of the dielectric β relaxation. It is conceivable that the hindrance exhibited by PTF in both intra and inter-molecular dynamics may play a role in the reduction of gas diffusion and permeability of PTF in comparison with PTT.

1. Introduction

The interest in the development of environmentally benign polymers is a long-time endeavor. Biodegradable and eventually biocompatible polymer materials have many potential applications in packaging and biomedicine among others. Pioneering research in bacterially produced polymers based in poly(3-hydroxybutyrate) (PHB) paved the way, time ago, for an industrial scale production of eco-friendly polymers [1–3]. More recently, fully biobased polyesters Poly(alkylene 2,5-furanoate)s, (PAF)s, based on 2,5-furandicarboxylic acid, have emerged as promising alternative to petroleum based poly(alkylene terephthalate)s [4,5]. Poly(ethylene 2,5-furandicarboxylate) (PEF) and poly(trimethylene 2,5-furandicarboxylate)(PTF) are typical counterparts of poly(ethylene terephthalate) (PET) and poly(trimethylene terephthalate)(PTT) respectively, widely used in packaging and fiber applications [4,6–8]. In addition to a lower production carbon footprint poly(alkylene 2,5-furanoate)s have received significant attention due to their outstanding gas barrier properties in comparison to traditional polyaromatic esters [8,9]. Systematic studies in PEF have been accomplished in order to understand the reason for the enhanced gas permeability of PAFs. Molecular modeling shows that π-π interactions of the furan rings favor the formation of compact helical conformations in the amorphous state of

* Corresponding author.
** Corresponding author.
E-mail addresses: oscar.galvez@ccia.uned.es (O. Gálvez), t.ezquerra@csic.es (T.A. Ezquerra).

https://doi.org/10.1016/j.polymer.2023.125699
Received 2 October 2022; Received in revised form 9 January 2023; Accepted 10 January 2023
Available online 13 January 2023

PAFs being related to their improved barrier properties [5,10]. Depending on processing conditions the presence of either a crystalline phase or a mesophase stabilized by hydrogen bonding (HB) has been shown to affect significantly the barrier properties of PAFs [8,11].

The influence of chain dynamics on barrier properties has also devoted some attention. Recent computer simulations indicate that ring-flipping chain dynamics has a significant impact on oxygen diffusion [12]. Previous experimental studies suggested that the sub-glass temperature relaxation processes influence gas diffusion. In particular, furan moiety in PEF hinders ring-flipping motions in comparison to benzene moiety of PET [9,13]. These late studies highlight the possible implication of chain dynamics in gas barrier properties. Although less investigated than PEF, PTF also exhibits significantly lower gas permeability values for O_2 and CO_2 than PET, PTT and its cycloaliphatic polymer counterparts [8,14,15]. PTF presents higher Young modulus and glass transition temperature than those of PTT while having a lower melting point. These properties make it attractive for commercial applications and industrial production [16].

Dielectric Spectroscopy has been used to characterize the molecular dynamics of PAFs [5,17–22]. By analyzing the relaxation time and the dielectric strength of the dielectric relaxation valuable information about the inter-molecular dynamics can be obtained [19,23]. Broadband Dielectric Spectroscopy (BDS) experiments performed in poly(trimethylene 2,5-furanoate)s revealed that the sub glass temperature relaxation (β), below its glass transition temperature [17] ($T_g = 53$ °C), exhibited inhibition of the mode corresponding to the ester oxygen linked to the aliphatic subunit which efficiently relaxes in the PTT ($T_g = 47$ °C) counterpart polymer [17,24]. It was proposed the single mode β relaxation to reflect restricted sub glass temperature dynamics in comparison to that of PTT contributing to the superior barrier performance exhibited by PTF [17].

Infrared (IR) spectroscopy is a widely used technique providing precise information of intra-molecular motions at the molecular level [23,25]. In addition to its common use as an analytical tool, IR spectroscopy has been used in polymers and in glass-forming liquids to investigate the glass transition, sub-glass dynamics and crystallization [26,27]. By evaluating the vibrational frequencies and the corresponding oscillator strength from the IR spectra, information about the intra-molecular dynamics can be available. It is worth mentioning that IR vibrational frequencies are orders of magnitude higher than the BDS ones, therefore, IR spectroscopy probes the local environment. The combination of IR spectroscopy and BDS can be an attractive approach to deal with molecular dynamics.

In this article, we present a combined IR spectroscopy and BDS study focused on the sub-glass temperature molecular dynamics of poly(trimethylene 2,5-furanoate) in comparison to that of poly(trimethylene terephthalate) in order to shed light on the potential influence of the dynamics on the barrier properties of Poly(alkylene 2,5-furanoate)s.

2. Experimental

2.1. Materials

Poly(trimethylene 2,5-furanoate) (PTF) ($M_n = 34.2\ 10^3$ g mol^{-1} and $Mw = 69.61\ 10^3$ g mol^{-1}) and poly(trimethylene terephthalate) (PTT) ($M_n = 34.46\ 10^3$ g mol^{-1}; $M_w = 70.72\ 10^3$ g mol^{-1}) were prepared by following a procedure as previously described elsewhere [28–30]. The chemical structure is shown in Scheme 1. In brief, PTF can be synthesized in two steps. The first step involves the transesterification reaction of 2,5-dimethyl furandicarboxylate (DMFDCA, Matrix Fine Chemicals, Switzerland) with bio-1,3-propanenediol (PDO, Susterra Propanediol, DuPont Tate & Lyle, USA) (DMFDCA/PDO molar ratio of 1:2). The reaction was held in a steel reactor at atmospheric pressure and under N_2 for 1 h at 165 °C in the presence of a catalyst (tetrabutyl orthotitanate (TBT, Fluka), 0.25 wt % in relation to FDCADM). In a second step, a polycondensation reaction takes place, in the presence of the same catalyst, at 230 °C for 1.5 h under a reduced pressure of 18 Pa. In this step, a thermal stabilizer is used (Irganox 1010, Ciba-Geigy, Switzerland, 0.5 wt% in relation to the final polymer mass).

Poly(trimethylene terephthalate)(PTT) was prepared by polycondensation in the molten state in two steps: i) transesterification of DMT by PDO in the presence of catalyst, and ii) polycondensation in the presence of the catalyst and thermal stabilizer. The reaction was carried out in the 1 L high pressure reactor (autoclave Engineers Pennsylvania, Erie, PA, USA) as previously described [24]. PTF and PTT can be then obtained by extrusion from the reactor under nitrogen, and cooling to room temperature in a water bath.

2.2. Sample preparation

Fourier Transform Infrared Spectroscopy (FTIR) spectroscopy was performed in polymer thin films prepared by spin-coating on FTIR transparent silicon substrates (Si FZ 25.4 mm Ø x 1 mm polished window). The polymers were solved in tri-fluoroacetic acid (SigmaAldrich, reagent grade ≥98%) with concentrations ranging from 20 g/L to 50 g/L. A fixed amount of 0.25 mL of the polymer solution was deposited by a syringe on the circular silicon substrate. A rotation speed of 2400 rpm was kept for 120 s. Spin-coated polymer films with thicknesses from about 200 nm to 900 nm can be easily obtained, depending on polymer concentrations, with an extremely flat surface, as measured by AFM [31]. The thickness of the films was controlled in order to have an efficient absorbance by FTIR spectroscopy with no saturation of bands. An optimal situation was obtained for films of 500–900 nm. According to FTIR performed in the spin-coated films, PTF is amorphous while PTT presents some bands associated with the crystalline phase (Figures S1, S2 and S3 in Supplementary Information). This was further corroborated by Grazing Incidence Wide Angle X-ray Scattering measurements (Fig. S4 in Supplementary Information). PTT spin-coated films typically exhibit a crystallinity of around 15% as previously described [31].

For BDS experiments amorphous thin polymer films, of about 200 μm in thickness, were obtained by compression molding of pellets above the melting temperature by using a hydraulic press (Dr. Collin GmbH,

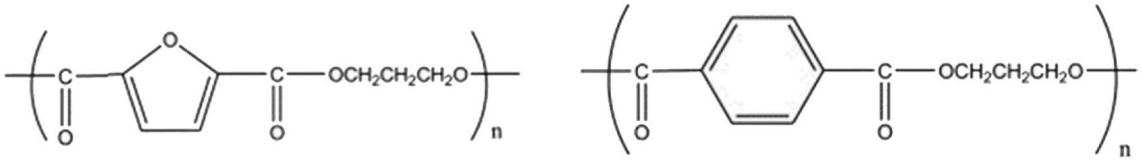

PTF PTT

Scheme 1. Chemical structure of poly(trimethylene 2,5-furanoate)(PTF) and poly(trimethylene terephthalate)(PTT).

Ebersberg, Germany) and subsequently cooled down in ice water. Pellets were dried for 24 h under vacuum at 60 °C before molding to eliminate water. This procedure typically produced amorphous films of PTT and PTF, as verified by Wide Angle X-ray Scattering, as previously published [17,24].

2.3. Ab initio calculation

In order to support infrared band assignment and experimental results, *ab initio* calculations were carried out for PTF and PTT monomers. Quantum mechanical calculations were performed with the Density Functional theory (DFT) method B3LYP which consists of Becke's three-parameter hybrid exchange functional [32] plus the nonlocal correlation functional of Lee, Yang, and Parr [33]. In addition, M06–2X functional which includes the D3 version of Grimme's dispersion has also been employed [34], mainly in the simulations of dimers of FDCA. We chose the aug-cc-pVTZ basis set as a reasonable compromise between size and reliability. A similar combination of the DFT method and basis set has been previously employed to evaluate the relative stability of PEF oligomers [5,10]. These calculations were computed using the Gaussian 16 software [35]. To simulate solid structures, periodic quantum chemical calculations were performed in the framework of the DFT by using the PBE exchange-correlation functional [36–38]. A DZP (doble zeta with polarization) basis set was chosen to provide a satisfactory flexibility for this kind of systems. These calculations were computed using the SIESTA (Spanish Initiative for Electronic Simulations with Thousands of Atoms) package [39]. In these calculations, the real space grid is fixed to 300 Ry.

2.4. Infrared spectroscopy and broadband Dielectric Spectroscopy experiments

FTIR spectra were acquired in vacuum (background pressure of 10^{-7} mbar) with a PerkinElmer, Frontier spectrometer in a 4500-500 cm^{-1} range with a resolution in the wavenumber of 2 and 4 cm^{-1}. The temperature range was varied between 20 K and 324 K by using a closed cycle He cryostat (CTI cryogenics). A spectrum for the background was taken at every temperature.

Complex dielectric permittivity (ε*) measurements ($\varepsilon^* = \varepsilon' - i\varepsilon''$) were performed over a frequency range of $10^{-1} < F/Hz < 10^6$ starting at T = 123 K up to room temperature by using a Novocontrol system integrating an ALPHA dielectric interface and QUATRO temperature control system (Novocontrol). Polymer films were sandwiched between two metallic electrodes of the spectrometer. The dielectric relaxations were empirically described in terms of the Havriliak-Negami (HN) equation [40]:

$$\varepsilon^* = \varepsilon' - i\varepsilon'' = \varepsilon_\infty + \frac{\Delta\varepsilon}{\left[1 + (i\omega\tau_{HN})^b\right]^c} \quad (1)$$

where ε′ the dielectric constant and ε'' the dielectric loss, Δε the dielectric strength, τ_{HN} is the central relaxation time of the relaxation time distribution function and ω is the angular frequency. The shape parameters b and c (0 < b, c < 1) describe the symmetric and the asymmetric broadening of the relaxation time distribution function, respectively.

3. Results and discussion

3.1. Fourier Transform Infrared Spectroscopy

Fig. 1a and b shows the FTIR absorption spectra of PTF and PTT at 300 K where absorption bands representative of significant molecular bonds have been highlighted. Tables S1 and S2 in the Supplementary Information collect the different bands and the assignment of the normal modes of vibration associated with them. According to FTIR, PTF film is amorphous while PTT presents some bands associated with the crystalline phase (Figures S1, S2 and S3 in Supplementary Information). PTT spin-coated films typically exhibit a crystallinity of around 15% as previously described [31]. In this case, the comparative study has been restricted to the bands of the amorphous phase. The assignment was carried out based on our *ab-initio* calculations and on the previous literature [10,41,42]. The relative intensity of every band, calculated as the ratio between the absorbance of the respective band, to the absorbance of the most intense band was also estimated.

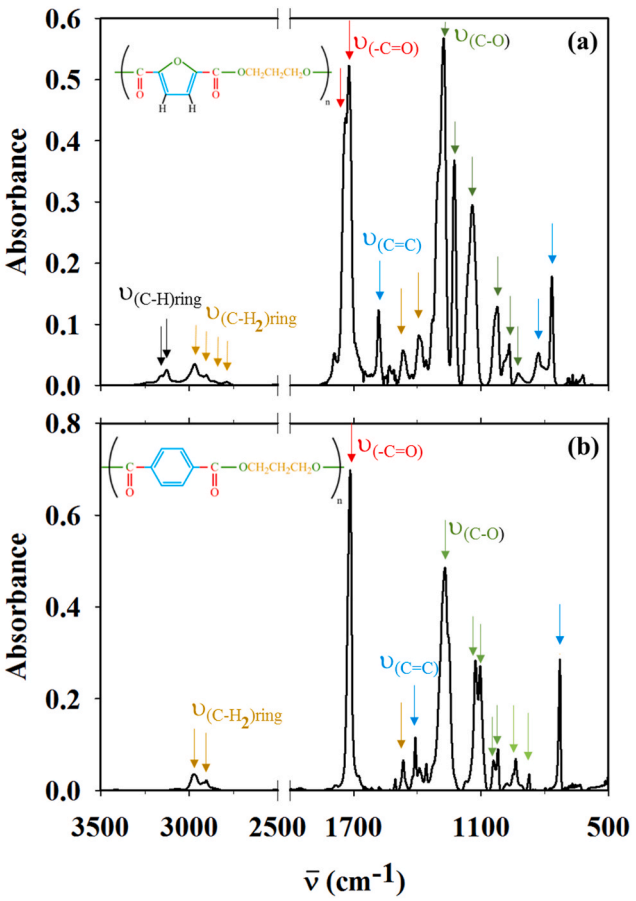

Fig. 1. FTIR absorption spectra of PTF (a) and PTT (b). The main chemical groups associated with the absorption features (ν stretching modes) are highlighted in the chemical structure of the polymers using the same color code as the arrows indicating the absorption bands in the spectra. (For interpretation of the references to color in this figure legend, the reader is referred to the Web version of this article.)

The temperature dependence of the FTIR spectra is rather weak in the investigated sub-glass temperature range in comparison with stronger variations observed upon crossing the glass transition temperature [23].

The temperature dependence of both, band positions and band areas, related to oscillator strength, of selected FTIR bands for PTF and PTT are shown in Figs. 2 and 3 respectively. Due to the sometimes subtle displacement with temperature of the bands, we have represented the magnitude $\Delta\bar{\nu} = \bar{\nu}_T - \bar{\nu}_{300\,K}$ (cm^{-1}), where $\bar{\nu}_T$ is the wavenumber of the selected band at a given temperature and $\bar{\nu}_{300\,K}$ at T = 300 K. Similarly for the band area, $\Delta A = \Delta A_T - \Delta A_{300K}$.

3.2. Broadband Dielectric Spectroscopy

Fig. 4a and b shows dielectric loss (ε'') data as a function of temperature and frequency for PTF and PTT respectively. The dielectric spectra are characterized by two main relaxations labelled as β and α.

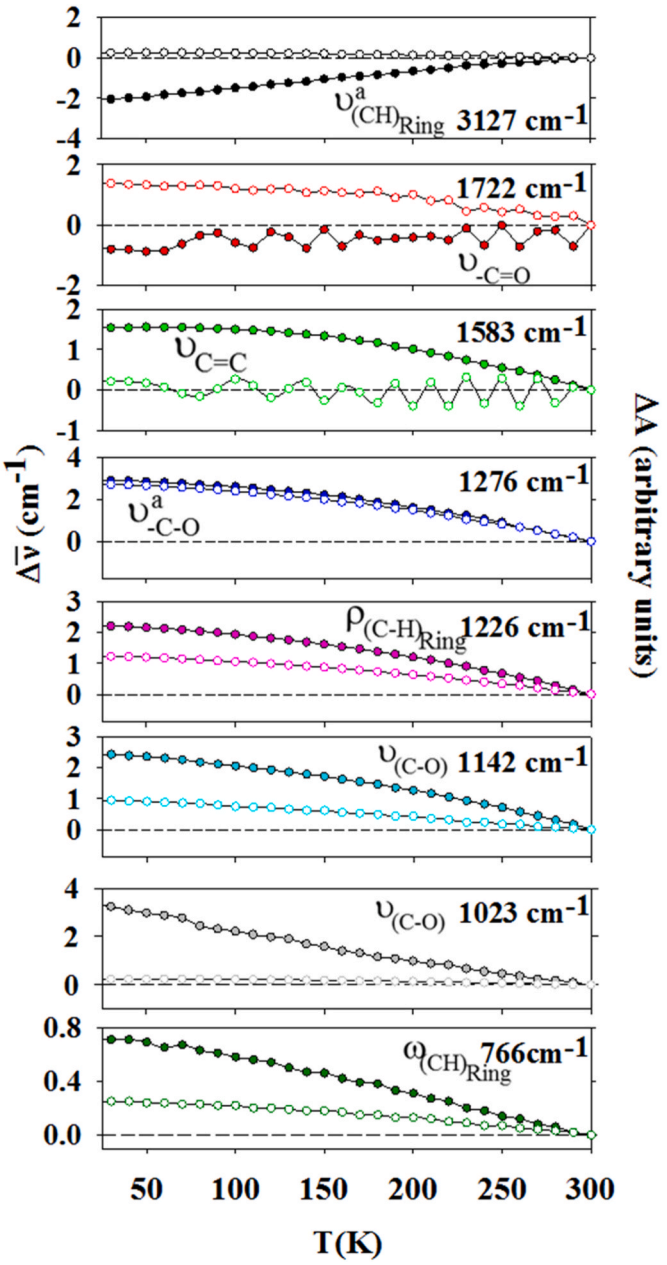

Fig. 2. $\Delta\bar{\nu} = \bar{\nu}_T - \bar{\nu}_{300\,K}$ (cm^{-1}) (full symbols, left axis) and area band (ΔA) (hollow symbols, right axis) as a function of temperature for selected IR bands of PTF. Short-dashed line is the $\bar{\nu} = 0$ reference. PTF bands: (•,o) 3127 cm^{-1} ($(C–H)_{ring}$ asymmetric stretching); (•,o) 1722 cm^{-1} (-C=O stretching); (•,o) 1583 cm^{-1} (C=C stretching); (•,o)1276 cm^{-1} (C–O asymmetric stretching); (•,o) 1226 cm^{-1} ($(C–H)_{ring}$ rocking, $(C–O)_{ring}$ stretching, C–O stretching); (•,o) 1142 cm^{-1} ($(C–H)_{ring}$ rocking, stretching, $(C–O)_{ring}$, C–O stretching), (•,o)1023 cm^{-1} ($(C–H)_{ring}$ rocking, $(C–O)_{ring}$ stretching, C–O stretching); (•,o) 766 cm^{-1} (wagging $(C–H)_{ring}$).

The α relaxation appears at temperatures above the glass transition and is related to the segmental dynamics [43]. Above the glass transition the polymers crystallize as revealed by the appearance of a second α-process, α_c, associated with segmental motions of the amorphous phase in the restricted environment induced by the crystalline phase as extensively described elsewhere [44–46]. Below the glass transition, in this case at sub-ambient temperatures, the most streaking fact is that while PTT exhibits two sub-glass temperature relaxation processes, β_1 and β_2, PTF exhibits a β relaxation of monomodal character as previously reported [5,17]. These differences in the β relaxation between PTF and

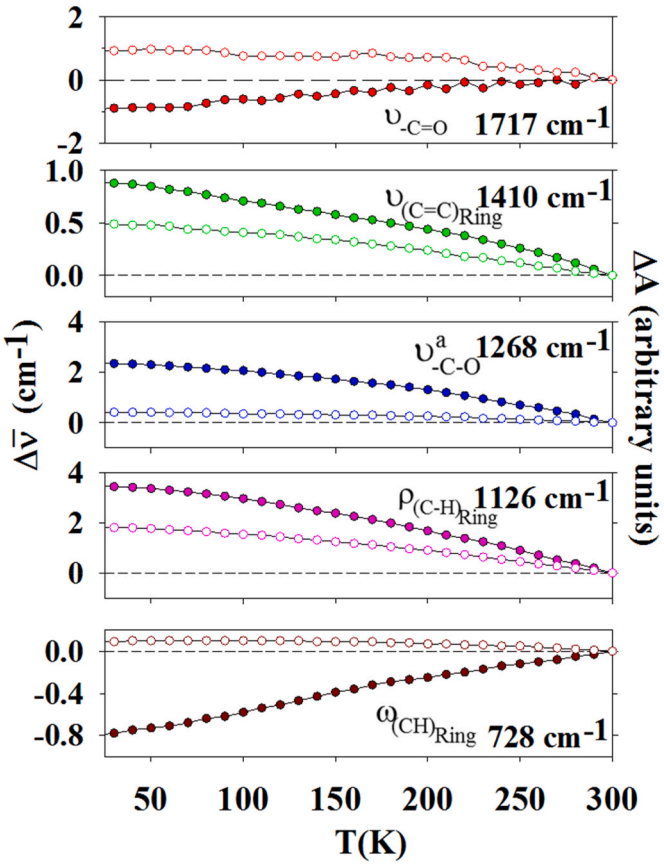

Fig. 3. $\Delta\bar{\nu} = \bar{\nu}_T - \bar{\nu}_{300\,K}$ (cm^{-1}) (full symbols, left axis) and area band (ΔA) (hollow symbols, right axis) as a function of temperature for selected IR bands of PTT. Short-dashed line is the $\Delta\nu = 0$ reference. PTT bands: (•,o) 1717 cm^{-1} (-C=O stretching); (•,o) 1410 cm^{-1} ($(C–C)_{ring}$ stretching, $(CH)_{ring}$ in-plane deformation); (•,o) 1268 cm^{-1} (C–O asymmetric stretching,$(CH)_{ring}$ rocking), (•,o) 1126 cm^{-1} ($(CH)_{ring}$ rocking, C–O Asymmetric stretching); (•,o) 728 cm^{-1} ($(C–H)_{ring}$ wagging).

PTT can be better visualized in the isothermal plots shown in Fig. 5. The β relaxation is related to the local dynamics of the different chemical bonds present in the polymer chain [24,47].

3.3. Inter and intra-molecular dynamics

The multimodal character of the subglass β relaxation has been described in detail for several aromatic polyesters [17,47–49]. Molecular dynamics simulations based on HBB force field model [50,51] propose that ester oxygen to aliphatic carbon bonds contribute to the fastest dynamics, β_1, while the relaxation of the aromatic ring carbon to ester carbon bond is related to the relaxation of the slower, β_2. It was suggested the higher rigidity, higher polarity and hindering of ring-flipping of the furan ring in comparison to the terephthalic aromatic ring [9,13] to have an impact on the local dynamics [17–19]. The wavenumbers and areas for FTIR bands for PTT (Fig. 3) exhibit a smooth non-linear temperature dependence. This type of weak temperature dependence has been observed in polystyrene [27] and other glass forming liquids [23] at temperatures below T_g. The shifts in wavenumber can be attributed to three main effects [23]: i) bond expansion, ii) bulk expansion and iii) conformational changes. In the subglass regime, below T_g, bond expansion should be the most significant causing a reduction of frequency (red-shift) with increasing temperature due to an increment of vibrational anharmonicities. The quantitative interpretation of the results requires quantum mechanical modeling that will be discussed in the next section. A qualitative similar tendency

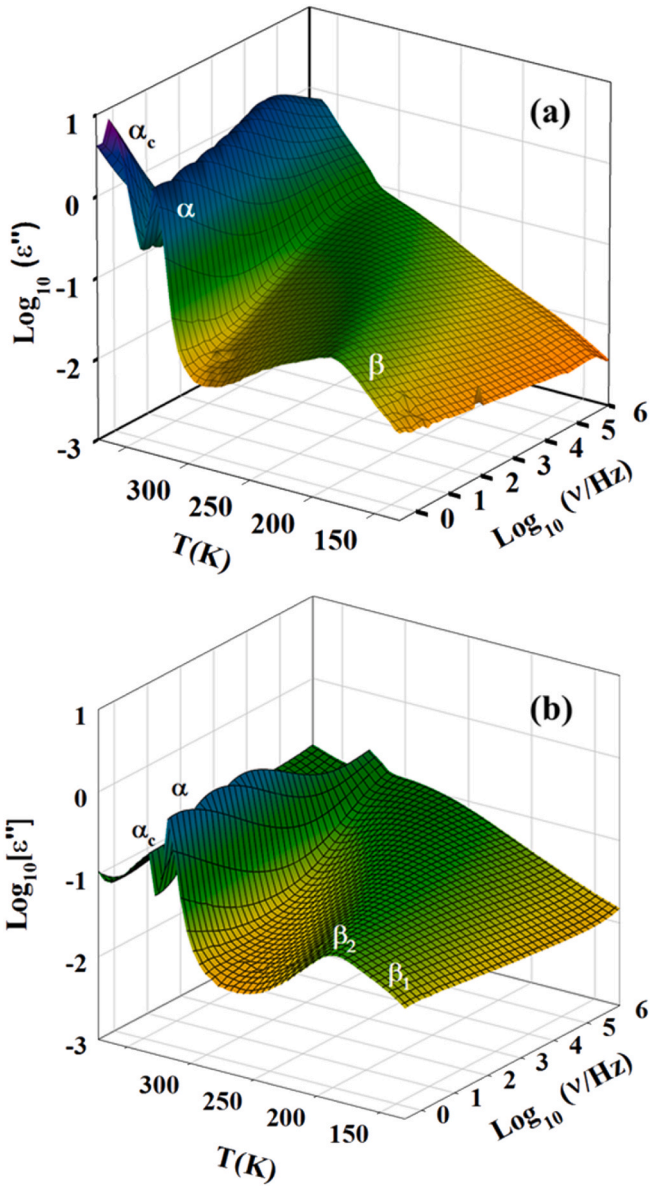

Fig. 4. Dielectric loss data, ε'', versus temperature (T) and frequency (ν) for: (a) PTF and (b) PTT.

(red-shifts with increasing temperature) is observed for the temperature dependence of the wavenumbers of FTIR bands of PTF (Fig. 2) with exception of those at 3127 cm^{-1} ((C–H)$_{ring}$ asymmetric stretching) and at 1722 cm^{-1} (-C═O stretching).

Fig. 6 represents vibrational wavenumbers and band areas for selected comparable FTIR bands of PTF and PTT as a function of the temperature. In addition, Fig. 7 compares the shape of the bands associated with the stretching of the carbonyl group for both polymers. The evolution with increasing temperature of comparable FTIR bands (Fig. 6) shows that both, PTF and PTT FTIR bands exhibit small red-shifts with exception of the band related to the stretching of the carbonyl group. There are no significant differences upon comparing PTF and PTT although it is worth mentioning that the band associated with C–O stretchings, 1276 cm^{-1} for PTF, exhibits around twice as much temperature dependence that the corresponding one for PTT at 1268 cm^{-1}. However, a significant difference appears in the shape of the bands associated with the C═O stretching (Fig. 7). While for PTT the band exhibits a single amorphous component for PTF is comprised of several ones.

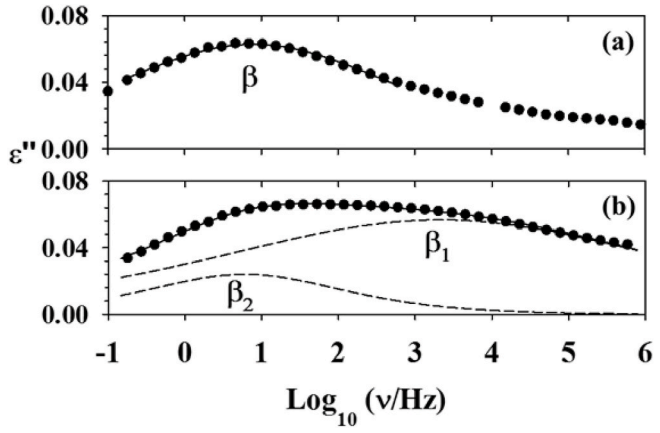

Fig. 5. Isothermal (T = 203 K) dielectric loss data (ε'') versus frequency (ν) for: (a) PTF and (b) PTT. The continuous lines represent the fit to the HN equation. Dashed lines correspond to the separate contribution of two components of the β relaxation for PTT.

The carbonyl C═O band is known to be very sensitive to both intermolecular and intramolecular interactions. For poly(vinyl acetate) adsorbed on silica particles and for polyfuranoates reinforced with nanoadditives the analysis of this band was exploited to probe the polymer/additive interface [52–54]. In our case, a similar analysis has been accomplished for both, the C═O bands of PTT and PTF. As illustrated in Fig. 7, the C═O band of PTT can be deconvoluted by two main contributions separated by only 6 cm^{-1} (1721 and 1715 cm^{-1}), and a very small contribution at 1784 cm^{-1} that could be assigned to non-bonded C═O. According to the previous literature, the main peaks can be ascribed to either amorphous (1721 cm^{-1}) or crystalline (1715 cm^{-1}) phases [42,55]. Regarding this analysis, the fraction of the crystalline PTT at 300 K could be estimated to be around 14%, a typical value for spin-coated films as mentioned above [31].

In the case of PTF, the C═O band reveals three main absorptions at 1792, 1744 and 1721 cm^{-1}. The high-frequency peak could be assigned to non-bonded C═O (as in the case of PTT). According to our calculations, that will be discussed in the next paragraph, the absorptions at 1744 and 1721 cm^{-1} can tentatively be ascribed to syn and anti conformations, respectively.

3.4. Quantum mechanical molecular simulation

As aforementioned, to gain further insight into the intra-molecular dynamics of PTF and PTT we have performed quantum mechanical calculations (both in vacuum and solid structures). PTF repeating unit is composed of two elements, namely: 1,3-propanediol (PG) and 2,5-furandicarboxylic acid (FDCA), shown in Fig. 8 (first row). Likewise, PTT is composed of PG and terephthalic acid (TEREPH) (Fig. 8, second row).

Previous studies for poly(ethylene 2,5-furanoate) (PEF) predict that, in the amorphous state, "gauche" structures of ethylene glycol (EG) and "anti" conformations of FDCA are energetically favoured [5,10]. The "syn" and "anti" conformations refer to the C═O group pointing to either the same or the opposite side than the oxygen atom of the furan ring, respectively. Fig. 8 shows "syn-syn", "syn-anti" and "anti-anti" conformations of the FDCA moiety.

In the case of propylene glycol (PG), several possibilities of gauche and trans configurations could be obtained (see two of them in Fig. 8). In PG, two C–C simple bonds are present, so firstly four combinations of gauche or trans configurations could be arranged, namely: TT, TG, GT and GG (G for gauche and T for trans). In addition, gauche conformations are achieved by clockwise (G$^+$) or anticlockwise (G$^-$) rotations around a simple C–C bond, even more, a simple O–C bond could also rotate to generate trans or gauche conformers (which can be labelled as: t, g$^+$ or g$^-$). The combination of a significant number of PG conformers

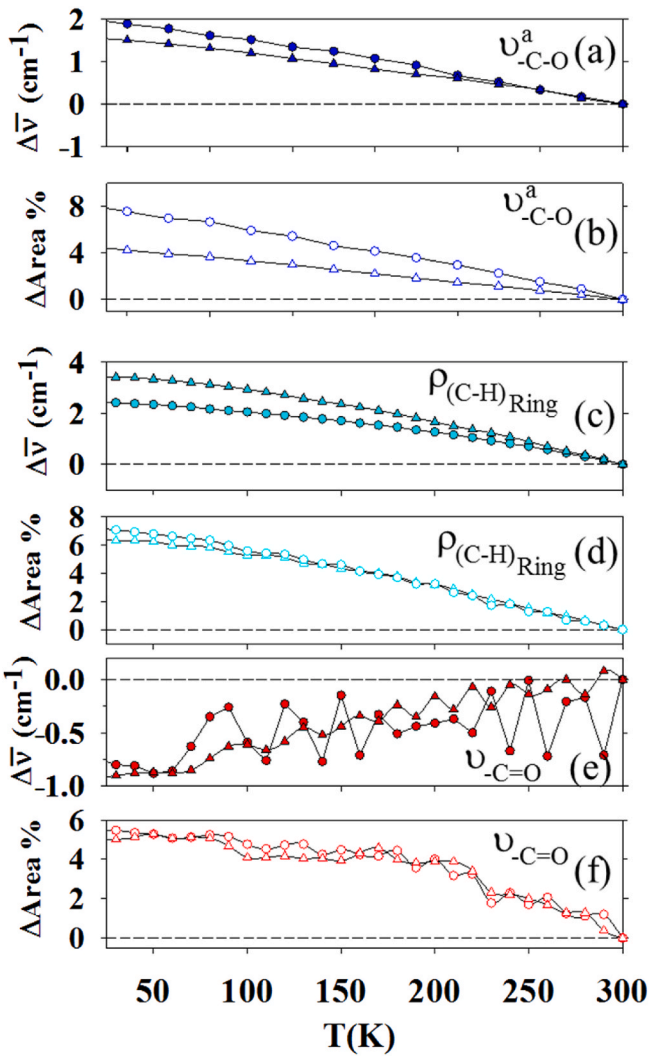

Fig. 6. Temperature dependence of $\Delta\,\bar{\nu} = \bar{\nu}_T - \bar{\nu}_{300\,K}$ (cm^{-1}) (bold symbols) and ΔArea (%) (open symbols) for selected comparable FTIR bands of PTF (circles) and PTT (triangles). **(a** and **b)** (•) 1276 cm^{-1} (**PTF C–O asymmetric stretching**) (▲) 1268 cm^{-1} (**PTT C–O asymmetric stretching**, $(CH)_{ring}$ rocking). **(c** and **d)**: (•) 1143 cm^{-1} (**PTF $(C–H)_{ring}$ rocking**, $(C–O)_{ring}$ stretching, C–O stretching), (▲) 1126 cm^{-1} (**PTT $(C–H)_{ring}$ rocking**, C–O asymmetric stretching). **(e** and **f)**:(●) 1722 cm^{-1} (PTF –C═O stretching), (▲) 1717 cm^{-1} (PTT –C═O stretching). Short-dashed line is the $\bar{\nu} = 0$ reference.

with the four possible FDCA conformers (syn-syn, syn-anti, anti-syn and anti-anti), results in a large landscape of structures just for a simple FDCA-PG unit. For this reason, to explore the full conformational space of PTF in order to postulate possible structures to be present in the amorphous phase is out of the scope of this study. Table S3 (Supplementary Information) shows the relative energy, in kcal/mol, of different isomers of FDCA, TEREPH and PG. Energy calculations by the DFT method predict the FDCA syn-syn configuration to be < 1 kcal/mol less stable than the anti-anti configuration in agreement with previous studies [5,10,56]. In the case of PG, all trans structure, tTTt, is only at ca. 1 kcal/mol from the tG⁻G⁻t conformation. Accordingly, syn-*syn*-trans isomers of PTF monomer are found to be only at a few kcal/mol from the most stable anti-*anti*-gauche configurations, according to our calculations. It is worth to mention that, at 160 K, RT is around 0.32 kcal/mol suggesting that the internal conversion of anti-gauche to syn-trans conformations in PTF could occur even at low temperatures. In the temperature evolution of the FTIR spectra of PTF we observe a continuous shift (red or blue) of the band positions and a monotonic decrease

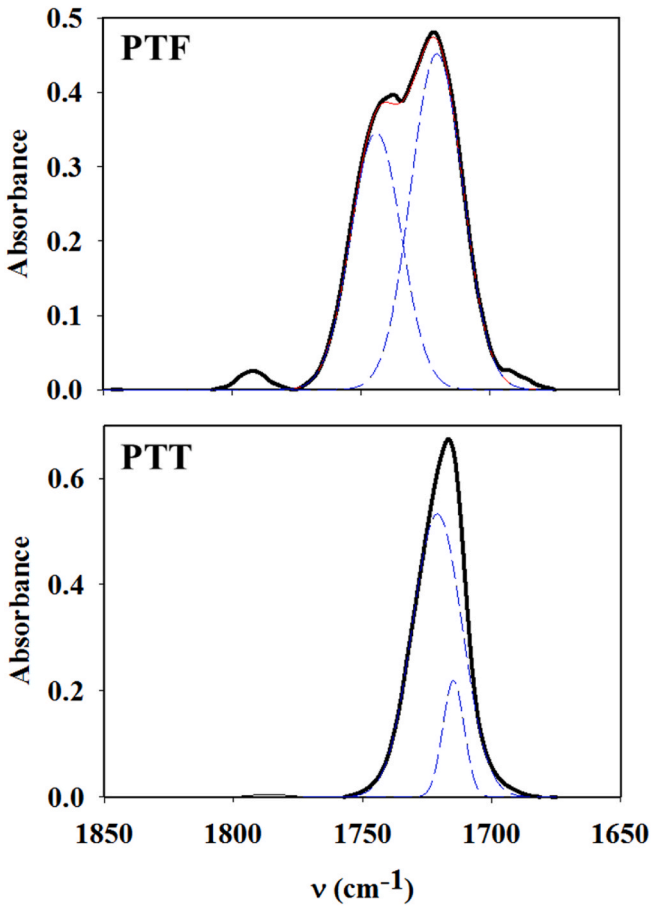

Fig. 7. FTIR absorption spectra of PTF and PTT at 300 K in the spectral region of the C═O stretching band.

of the band area with increasing temperature. The red-shift of the bands can be explained by a continuous bond expansion causing a reduction of the frequency with increasing temperature due to an increment of vibrational anharmonicities. In order to shed some light on this behaviour, we focused on the following modes: i) –C═O stretching (around 1722 cm^{-1}) and ii) C═C stretching (1583 cm^{-1}) because these bands are key infrared features with opposite tendencies in their temperature dependences (see Fig. 2). In addition, these bands present a major contribution of C═O or C═C bonds with the insignificant influence of other modes. Table 1 shows that calculated wavenumbers of C═O and C═C stretching modes of FDCA are in fair agreement with the observed IR absorption peaks. Moreover, the agreement is better for the case of anti-anti conformer especially for C═O stretching. This is the most favourable conformation in the amorphous phase [10]. Regarding the changes predicted for different conformers, the C═O stretching frequency is blue-shifted around 27 or 18 cm^{-1} (for symmetric and asymmetric stretching mode, respectively) from anti-anti to syn-syn configuration in FDCA. In contrast, C═C stretching frequency is red-shifted 13 cm^{-1} from anti-anti to syn-syn isomer. As mentioned previously and according to these calculations, the observed multimodal C═O band of PTF is suggested to be mainly formed by contributions from syn and anti conformations in the amorphous phase.

Accordingly, we can hypothesize that as temperature increases, the observed blue-shift of the C═O stretching band and concurrent red-shift of the C═C stretching band would be expected if an increment of the syn-syn conformations takes place. The evolution from more stable anti-anti to less stable syn-syn isomers can be compensated by the occurrence of HB between interchain FDCA moieties in syn-syn conformations. In particular, FTIR bands corresponding to stretching modes of the

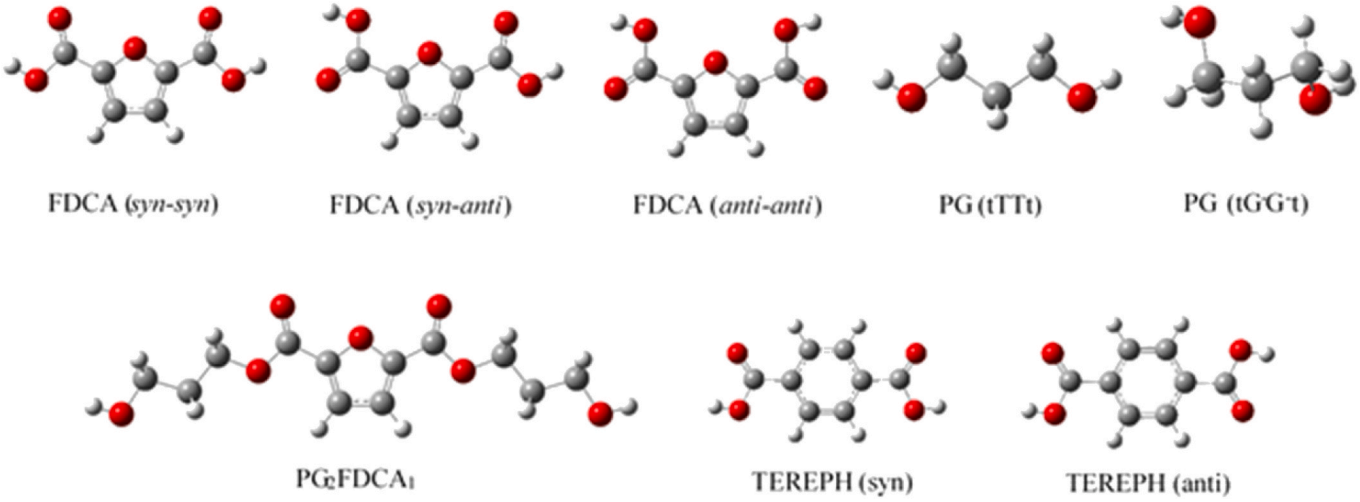

Fig. 8. Molecular structure of FDCA, PG, PG_2FDCA_1 and TEREPH compounds. Optimized at B3LYP/aug-cc-pVTZ.

Table 1
Calculated band position (in cm^{-1}) for selected normal modes of FDCA, $FDCA_2$ and TEREPH (see Figs. 8 and 9) at M06–2X/aug-cc- pVTZ level. Calculated frequencies are scaled by a factor of 0.956 [57]. Bold is used to highlight the most intense band.

	C=O stretching *sym*	C=O stretching *asym*	C=C stretching
FDCA (*anti-anti*)	1774	**1765**	1591
FDCA (*syn-anti*)	1790	**1768**	1586
FDCA (*syn-syn*)	**1801**	1783	1578
$FDCA_2$ (HB)	1798, **1791**	1775, **1772**	1579, 1574
$FDCA_2$ (π–π)	**1813**, 1805	**1783,** 1744	**1576**, 1574
Observed[a]	1722		1583
TEREPH (*syn*)	**1773**	1769	
TEREPH (*anti*)	1773	**1767**	
Observed[a]	1717		

[a] Observed band position for amorphous PTF or PTT at 300 K.

$(C–H)_{ring}$ and of the (-C═O) bonds are particularly sensitive to the formation of hydrogen bonds [10]. As mentioned above, these two bands exhibit a blue-shift with increasing temperature (Fig. 2). In order to evaluate the role of hydrogen bond interaction and π–π stacking, different configurations of FDCA dimers have been simulated as shown in Fig. 9. Relative energies and relevant structural parameters are collected in Table 2. In this case, calculations were performed at M06–2X/aug-cc-pVTZ. M06–2X functional including the D3 version of Grimme's dispersion as it resulted more appropriate to account for the intermolecular interactions present in these systems [5].

As it is shown in Table 2, the formation of HB and π–π interactions provide an extra stabilization to the system. However, π–π interactions cause lower ΔE values than hydrogen bonding, even though larger intermolecular distances are obtained. The carbonyl stretching C═O mode is highly sensitive to both intermolecular and intramolecular changes, and according to our calculations, the formation of the intermolecular C–H···O bonds promotes an additional red-shift of ca. 10 cm^{-1}

Table 2
$\Delta E_{dimer} = E_{dimer} - 2 \times E_{monomer}$ in kcal/mol (zero-point vibrational energy and thermal corrections included) for dimers of FDCA shown in Fig. 9, calculated at M062X/aug-cc-pVDZ. Distances are given in Å.

	$FDCA_2$ (HB)	$FDCA_2$ (π-π)
ΔE_{dimer}	−3.02	−4.56
d(C═O···H)	2.328	
d(π···π)		3.330
Crystal[a]	2.47	3.39

[a] Observed values in Ref. [56] for PEF in which d(π···π) is the distance between planes.

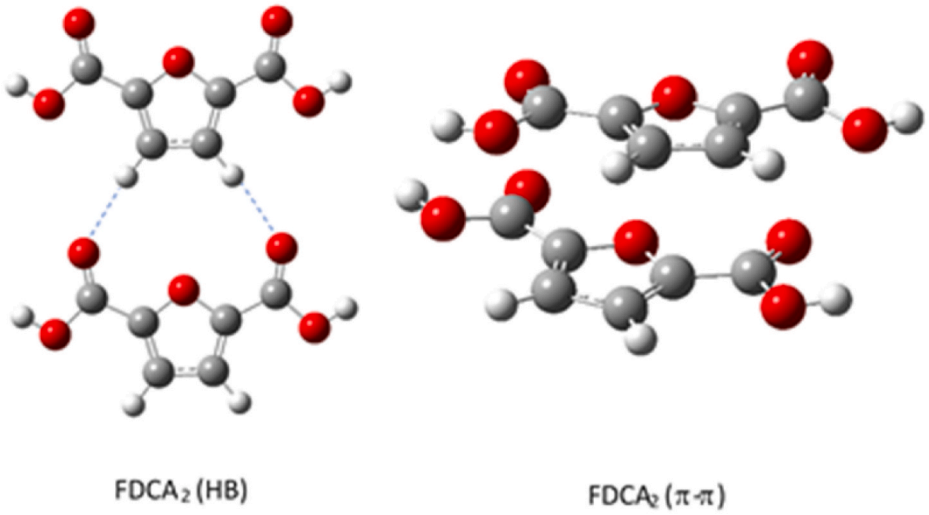

Fig. 9. Molecular structures of two conformers of a dimer of FDCA. Optimized at M062X/aug-cc-pVTZ.

(see Table 1) for the syn-syn conformation. In addition, a blue-shift is predicted for C═O stretching when π–π stacking interactions are formed. Thus, these competing effects could provoke that the additional changes in the C═O stretching band during anti-anti to syn-syn isomerization as temperature increases are lower than those found for C═C band as observed in our spectra. For PEF, the multimodality of this band has been attributed to the presence of hydrogen bonding [10]. In our case for PTF, the X-ray diffractograms (Fig. S4, Supplementary Information) of the investigated spin-coated films reveals the presence of a bump in the amorphous halo, marked with an arrow. Previous studies have shown in thicker films of PTF and of poly(pentamethylene 2,5-furanoate)(PPeF) prepared by compression molding the presence of a sharp maximum, in a similar range, which has been interpreted as due to the existence of an HB network [8,11].

For the case of PTT, two structures of the element TEREPH are predicted, namely "syn" and "anti". Both configurations are isoenergetic, according to our DFT calculations (see Table S3). The calculated C═O stretching modes wavenumbers are also similar for both conformations (see Table 1). Although the different intensity values for the asymmetric and symmetric mode could arise in a multimodal C═O band, the observed amorphous peak (Fig. 7b) could indicate that only a type of conformer is formed, as occur for the crystalline structure which present only the "anti" conformation [58,59].

Finally, with the aim to also estimate the inter-chain interactions that take place in PTT, we have performed periodic quantum chemical calculations on the crystal structure of PTT [58] (see Fig. S5 and Table S4 in the supporting information). Our calculated unit cell parameters show a nice agreement with the experimental and previous studies (Table S4). In this crystalline structure, compared to the short H-bonds distances predicted between FDCA motifs of PTF (of ca. 2.33 Å in Table 2), much longer interchain contacts are formed (which implicate C═O groups and hydrogens from the aliphatic chain), ranging from 2.7 to 3.0 Å (see Fig. S5), which suggests that lower interactions energies occur in PTT than PTF.

In this respect, putting into context the dielectric β relaxation of PTF and PTT and the FTIR observations the formation of hydrogen bonding in the amorphous state of PTF may cause an additional hindrance for the intermolecular motions of the monomer inducing a monomodal β relaxation.

4. Conclusion

In summary, the temperature dependence in the glassy state of comparable FTIR bands is very similar for PTF and PTT and shows small red shifts, with exception of the band related to the stretching of the carbonyl group. A significant difference appears in the shape of the bands associated with the C═O stretching suggesting the presence of hydrogen bonds in amorphous PTF. This effect may be behind the monomodal shape of the beta relaxation of PTF due to a higher degree of intramolecular coupling between the furan ring and the rest of the monomer. Quantum mechanical calculations and FTIR analysis suggest that, as temperature increases, an increment of the syn-syn conformations of the 2,5-furandicarboxylic acid (FDCA) moiety is likely to occur in the amorphous state. The energetically unfavorable balance can be compensated by hydrogen bonding. This effect can provoke and additional hindrance for the intermolecular motions of the monomer inducing a monomodal dielectric beta relaxation. It is conceivable that this hindrance exhibited by PTF in both intra- and inter-molecular dynamics may play a role in the reduction of gas diffusion and permeability of PTF in comparison with PTT.

Author contributions

General concept and coordination (OG, TAE). Chemical synthesis (II, SP, AS). FTIR experiments (OG, MS, OT, FJH, ER, TAE). BDS experiments (II, AL, AN, MCGG, TAE). Manuscript preparation (OG, GS, TAE). All co-authors contributed equally to both, the discussion and the conclusions.

Funding sources

PID2019-107514 GB-I00/AEI/10.13039/501100011033 and PID2019-106125 GB-I00/AEI/10.13039/501100011033. SONATA no 2018/31/D/ST8/00792.

Declaration of competing interest

The authors declare that they have no known competing financial interests or personal relationships that could have appeared to influence the work reported in this paper.

Data availability

Data will be made available on request.

Acknowledgment

Grants PID2019-107514 GB-I00/AEI/10.13039/501100011033 and PID2019-106125 GB-I00/AEI/10.13039/501100011033 funded by MCIN/AEI/10.13039/501100011033 and by " ERDF A way of making Europe". GS acknowledges grant RYC2020-029810-I funded by MCIN/AEI/10.13039/501100011033 and by " ESF Investing in your future". SP would like to thank for financial support from the National Science Centre within project SONATA no 2018/31/D/ST8/00792. Authors acknowledge J.P. Sánchez for technical support and E. Solano for the GIWAXS experiments performed in NCD-SWEET beamline at ALBA synchrotron with the collaboration of ALBA staff.

Appendix A. Supplementary data

Supplementary data to this article can be found online at https://doi.org/10.1016/j.polymer.2023.125699.

References

[1] P.J. Barham, A. Keller, E.L. Otun, P.A. Holmes, Crystallization and morphology of a bacterial thermoplastic- poly-3-hydroxybutyrate, J. Mater. Sci. 19 (9) (1984) 2781–2794.
[2] J. Martinez de Salazar, M. Sanchez-Cuesta, P.J. Barham, A. Keller, Thermal-expansion and spherulite cracking in 3-Hydroxybutyrate 3-Hydroxyvalerate copolymers, J. Mater. Sci. Lett. 8 (4) (1989) 490–492.
[3] M. Sanchez-Cuesta, J. Martinez de Salazar, P.A. Barker, P.J. Barham, Cocrystallization of poly(3-hydroxybutyrate-co-3-hydroxyvalerate), J. Mater. Sci. 27 (19) (1992) 5335–5338.
[4] J.A. Moore, J.E. Kelly, Polyesters derived from furan and tetrahydrofuran nuclei, Macromolecules 11 (3) (1978) 568–573.
[5] G. Papamokos, T. Dimitriadis, D.N. Bikiaris, G.Z. Papageorgiou, G. Floudas, Chain conformation, molecular dynamics, and thermal properties of poly(n-methylene 2,5-furanoates) as a function of methylene unit sequence length, Macromolecules 52 (17) (2019) 6533–6546.
[6] A. Gandini, A.J.D. Silvestre, C.P. Neto, A.F. Sousa, M. Gomes, The furan counterpart of poly(ethylene terephthalate): an alternative material based on renewable resources, J. Polym. Sci. Polym. Chem. 47 (1) (2009) 295–298.
[7] G.Z. Papageorgiou, D.G. Papageorgiou, Z. Terzopoulou, D.N. Bikiaris, Production of bio-based 2,5-furan dicarboxylate polyesters: recent progress and critical aspects in their synthesis and thermal properties, Eur. Polym. J. 83 (2016) 202–229.
[8] G. Guidotti, M. Soccio, M.C. Garcia-Gutierrez, T. Ezquerra, V. Siracusa, E. Gutierrez-Fernandez, A. Munari, N. Lotti, Fully biobased superpolymers of 2,5-furandicarboxylic acid with different functional properties: from rigid to flexible, high performant packaging materials, ACS Sustain. Chem. Eng. 8 (25) (2020) 9558–9568.
[9] S.K. Burgess, R.M. Kriegel, W.J. Koros, Carbon dioxide sorption and transport in amorphous poly(ethylene furanoate), Macromolecules 48 (7) (2015) 2184–2193.
[10] C.F. Araujo, M.M. Nolasco, P.J.A. Ribeiro-Claro, S. Rudic, A.J.D. Silvestre, P. D. Vaz, A.F. Sousa, P.E.F. Inside, Chain conformation and dynamics in crystalline and amorphous domains, Macromolecules 51 (9) (2018) 3515–3526.
[11] G. Guidotti, M. Soccio, M.C. Garcia-Gutierrez, E. Gutierrez-Fernandez, T. A. Ezquerra, V. Siracusa, A. Munari, N. Lotti, Evidence of a 2D-ordered structure in biobased poly(pentamethylene furanoate) responsible for its outstanding barrier and mechanical properties, ACS Sustain. Chem. Eng. 7 (21) (2019) 17863–17871.

[12] J.C. Lightfoot, A. Buchard, B. Castro-Dominguez, S.C. Parker, Comparative study of oxygen diffusion in polyethylene terephthalate and polyethylene furanoate using molecular modeling: computational insights into the mechanism for gas transport in bulk polymer systems, Macromolecules 55 (2) (2022) 498–510.
[13] S.K. Burgess, J.E. Leisen, B.E. Kraftschik, C.R. Mubarak, R.M. Kriegel, W.J. Koros, Chain mobility, thermal, and mechanical properties of poly(ethylene furanoate) compared to poly(ethylene terephthalate), Macromolecules 47 (4) (2014) 1383–1391.
[14] M. Vannini, P. Marchese, A. Celli, C. Lorenzetti, Fully biobased poly(propylene 2,5-furandicarboxylate) for packaging applications: excellent barrier properties as a function of crystallinity, Green Chem. 17 (8) (2015) 4162–4166.
[15] G. Guidotti, L. Genovese, M. Soccio, M. Gigli, A. Munari, V. Siracusa, N. Lotti, Block copolyesters containing 2,5-furan and trans-1,4-cyclohexane subunits with outstanding gas barrier properties, Int. J. Mol. Sci. 20 (9) (2019) 2187–2201.
[16] A. Tullo, Renewable Chemistry: low-cost route enables a sugar-derived plastic, C&EN Glob. Enterp. 94 (2016), 6-6.
[17] L. Genovese, M. Soccio, N. Lotti, A. Munari, A. Szymczyk, S. Paszkiewicz, A. Linares, A. Nogales, T.A. Ezquerra, Effect of chemical structure on the subglass relaxation dynamics of biobased polyesters as revealed by dielectric spectroscopy: 2,5-furandicarboxylic acid vs. trans-1,4-cyclohexanedicarboxylic acid, Phys. Chem. Chem. Phys. 20 (23) (2018) 15696–15706.
[18] C. Fosse, A. Esposito, S. Thiyagarajan, M. Soccio, N. Lotti, E. Dargent, L. Delbreilh, Cooperativity and fragility in furan-based polyesters with different glycolic subunits as compared to their terephthalic counterparts, J. Non-Cryst. Solids 597 (2022) art. number 121907.
[19] A. Bourdet, A. Esposito, S. Thiyagarajan, L. Delbreilh, F. Affouard, R.J.I. Knoop, E. Dargent, Molecular mobility in amorphous biobased poly(ethylene 2,5-furan-dicarboxylate) and poly(ethylene 2,4-furandicarboxylate), Macromolecules 51 (5) (2018) 1937–1945.
[20] M. Soccio, D.E. Martinez-Tong, A. Alegria, A. Munari, N. Lotti, Molecular dynamics of fully biobased poly(butylene 2,5-furanoate) as revealed by broadband dielectric spectroscopy, Polymer 128 (2017) 24–30.
[21] T. Dimitriadis, D.N. Bikiaris, G.Z. Papageorgiou, G. Floudas, Molecular dynamics of poly(ethylene-2,5-furanoate) (PEF) as a function of the degree of crystallinity by dielectric spectroscopy and calorimetry, Macromol. Chem. Phys. 217 (18) (2016) 2056–2062.
[22] A. Bourdet, S. Araujo, S. Thiyagarajan, L. Delbreilh, A. Esposito, E. Dargent, Molecular mobility in amorphous biobased copolyesters obtained with 2,5-and 2,4-furandicarboxylate acid, Polymer 213 (2021) art. number 123225.
[23] F. Kremer, W. Kossack, A.M. Anton, Glassy dynamics as reflected in the inter- and intra-molecular interactions, in: F. Kremer, A. Loidl (Eds.), The Scaling of Relaxation Processes. Advances in Dielectrics Springer, 2018.
[24] I. Irska, S. Paszkiewicz, D. Pawlikowska, J. Dryzek, A. Linares, A. Nogales, T. A. Ezquerra, E. Piesowicz, Relaxation behaviour and free volume of bio-based Poly (trimethylene terephthalate)-block-poly(caprolactone) copolymers as revealed by Broadband Dielectric and Positron Annihilation Lifetime Spectroscopies, Polymer 229 (2021) art. number 123949.
[25] F. Kremer, W.K. Kipnusu, M. Fraenzl, Orientation polarization spectroscopy-toward an atomistic understanding of dielectric relaxation processes, Int. J. Mol. Sci. 23 (15) (2022) art. number 8254.
[26] P. Papadopoulos, W. Kossack, F. Kremer, Intra- and inter-molecular dynamics in glass-forming liquids, Soft Matter 9 (5) (2013) 1600–1603.
[27] W. Kossack, M. Schulz, T. Thurn-Albrecht, J. Reinmuth, V. Skokow, F. Kremer, Temperature-dependent IR-transition moment orientational analysis applied to thin supported films of poly-epsilon-caprolactone, Soft Matter 13 (48) (2017) 9211–9219.
[28] S. Paszkiewicz, A. Szymczyk, I. Irska, D. Pawlikowska, E. Piesowicz, Synthesis, structure, and physical properties of poly(trimethylene terephthalate)-block-poly (caprolactone) copolymers, J. Appl. Polym. Sci. 136 (15) (2019), 47341-47341.
[29] M. Kwiatkowska, I. Kowalczyk, K. Kwiatkowski, A. Szymczyk, Z. Roslaniec, Fully biobased multiblock copolymers of furan-aromatic polyester and dimerized fatty acid: synthesis and characterization, Polymer 99 (2016) 503–512.
[30] A. Zubkiewicz, A. Szymczyk, R.J. Sablong, M. Soccio, G. Guidotti, V. Siracusa, N. Lotti, Bio-based aliphatic/aromatic poly(trimethylene furanoate/sebacate) random copolymers: correlation between mechanical, gas barrier performances and compostability and copolymer composition, Polym. Degrad. Stabil. 195 (2022) art. number 109800.
[31] I. Martin-Fabiani, E. Rebollar, S. Perez, D.R. Rueda, M.C. Garcia-Gutierrez, A. Szymczyk, Z. Roslaniec, M. Castillejo, T.A. Ezquerra, Laser-induced periodic surface structures nanofabricated on poly(trimethylene terephthalate) spin-coated films, Langmuir 28 (20) (2012) 7938–7945.
[32] A.D. Becke, Denstity-functional exchange-energy approximation with correct asymptotic-behaviour, Phys. Rev. 38 (6) (1988) 3098–3100.
[33] C.T. Lee, W.T. Yang, R.G. Parr, Development of the Colle-Salvetti correlation-energy formula into a functional of the electron density, Phys. Rev. B 37 (2) (1988) 785–789.
[34] S. Grimme, J. Antony, S. Ehrlich, H. Krieg, A consistent and accurate ab initio parametrization of density functional dispersion correction (DFT-D) for the 94 elements H-Pu, J. Chem. Phys. 132 (15) (2010), 154104.
[35] M.J. Frisch, G.W. Trucks, H.B. Schlegel, G.E. Scuseria, M.A. Robb, J.R. Cheeseman, G. Scalmani, V. Barone, G.A. Petersson, H. Nakatsuji, X. Li, M. Caricato, A. V. Marenich, J. Bloino, B.G. Janesko, R. Gomperts, B. Mennucci, H.P. Hratchian, J. V. Ortiz, A.F. Izmaylov, J.L. Sonnenberg, Williams, F. Ding, F. Lipparini, F. Egidi, J. Goings, B. Peng, A. Petrone, T. Henderson, D. Ranasinghe, V.G. Zakrzewski, J. Gao, N. Rega, G. Zheng, W. Liang, M. Hada, M. Ehara, K. Toyota, R. Fukuda, J. Hasegawa, M. Ishida, T. Nakajima, Y. Honda, O. Kitao, H. Nakai, T. Vreven, K. Throssell, J.A. Montgomery Jr., J.E. Peralta, F. Ogliaro, M.J. Bearpark, J. J. Heyd, E.N. Brothers, K.N. Kudin, V.N. Staroverov, T.A. Keith, R. Kobayashi, J. Normand, K. Raghavachari, A.P. Rendell, J.C. Burant, S.S. Iyengar, J. Tomasi, M. Cossi, J.M. Millam, M. Klene, C. Adamo, R. Cammi, J.W. Ochterski, R.L. Martin, K. Morokuma, O. Farkas, J.B. Foresman, D.J. Fox, Gaussian 16, Rev. C.01, Wallingford, CT, 2016.
[36] J.P. Perdew, K. Burke, M. Ernzerhof, Generalized gradient approximation made simple, Phys. Rev. Lett. 77 (18) (1996) 3865–3868.
[37] J.P. Perdew, K. Burke, M. Ernzerhof, Generalized gradient approximation made simple (vol 77, pg 3865, Phys. Rev. Lett. 78 (7) (1996), 1997) 1396-1396.
[38] K. Berland, P. Hyldgaard, Exchange functional that tests the robustness of the plasmon description of the van der Waals density functional, Phys. Rev. B 89 (3) (2014) art. number 035412.
[39] J.M. Soler, E. Artacho, J.D. Gale, A. Garcia, J. Junquera, P. Ordejon, D. Sanchez-Portal, The SIESTA method for ab initio order-N materials simulation, J. Phys. Condens. Matter 14 (11) (2002) 2745–2779.
[40] S. Havriliak, S. Negami, On equivalence of dielectric and mechanical dispersions in some polymers-eg poly(normal-octyl methacrylate), Polymer 10 (11) (1969) 859–872.
[41] A. Zubkiewicz, I. Irska, P. Miadlicki, K. Walkowiak, Z. Rozwadowski, S. Paszkiewicz, Structure, thermal and mechanical properties of copoly(ester amide)s based on 2,5-furandicarboxylic acid, J. Mater. Sci. 56 (34) (2021) 19296–19309.
[42] I.M. Ward, M.A. Wilding, IR and Raman.spectra of poly(m-methylene terephthalate) polymers, Polymer 18 (4) (1977) 327–335.
[43] F. Kremer, A. Schonhals, Broadband Dielectric Spectroscopy, Springer Verlag, Heidelberg, Germany, 2002.
[44] A. Nogales, T.A. Ezquerra, J.M. Garcia, F.J. Balta-Calleja, Structure-dynamics relationships of the alpha-relaxation in flexible copolyesters during crystallization as revealed by real-time methods, J. Polym. Sci. B Polym. Phys. 37 (1) (1999) 37–49.
[45] A. Sanz, A. Nogales, T.A. Ezquerra, N. Lotti, A. Munari, S.S. Funari, Order and segmental mobility during polymer crystallization: poly (butylene isophthalate), Polymer 47 (4) (2006) 1281–1290.
[46] T.A. Ezquerra, A. Nogales, Crystallization as studied by broadband dielectric spectroscopy, in: F. Kremer (Ed.), Advances in Dielectrics, Springer Heidelberg, Germany, 2020.
[47] M. Soccio, A. Nogales, T.A. Ezquerra, N. Lotti, A. Munari, Effect of copolymerization in the dynamics of poly(trimethylene terephthalate), Macromolecules 45 (1) (2012) 180–188.
[48] I. Martin-Fabiani, A. Linares, A. Nogales, T.A. Ezquerra, Dielectric relaxation of poly (trimethylene terephthalate) in a broad range of crystallinity, Polymer 54 (21) (2013) 5892–5898.
[49] S.P. Bravard, R.H. Boyd, Dielectric relaxation in amorphous poly(ethylene terephthalate) and poly(ethylene 2,6-naphthalene dicarboxylate) and their copolymers, Macromolecules 36 (3) (2003) 741–748.
[50] S.U. Boyd, R.H. Boyd, Chain dynamics and relaxation in amorphous poly(ethylene terephthalate): a molecular dynamics simulation study, Macromolecules 34 (20) (2001) 7219–7229.
[51] M.S. Hedenqvist, R. Bharadwaj, R.H. Boyd, Molecular dynamics simulation of amorphous poly(ethylene terephthalate), Macromolecules 31 (5) (1998) 1556–1564.
[52] M. Fullbrandt, P.J. Purohit, A. Schonhals, Combined FTIR and dielectric investigation of poly(vinyl acetate) adsorbed on silica particles, Macromolecules 46 (11) (2013) 4626–4632.
[53] P.A. Klonos, L. Papadopoulos, G.Z. Papageorgiou, A. Kyritsis, P. Pissis, D. N. Bikiaris, Interfacial interactions, crystallization, and molecular dynamics of renewable poly(propylene furanoate) in situ filled with initial and surface functionalized carbon nanotubes and graphene oxide, J. Phys. Chem. C 124 (18) (2020) 10220–10234.
[54] P.A. Klonos, L. Papadopoulos, Z. Terzopoulou, G.Z. Papageorgiou, A. Kyritsis, D. N. Bikiaris, Molecular dynamics in nanocomposites based on renewable poly (butylene 2,5-furan-dicarboxylate) in situ reinforced by montmorillonite nanoclays: effects of clay modification, crystallization, and hydration, J. Phys. Chem. B 124 (33) (2020) 7306–7317.
[55] Z. Chen, S. Yan, Structural variation of melt-crystallized PTT during the heating process revealed by FTIR and SAXS, Chin. Sci. Bull. 58 (3) (2013) 328–335.
[56] Y. Mao, R.M. Kriegel, D.G. Bucknall, The crystal structure of poly(ethylene furanoate), Polymer 102 (2016) 308–314.
[57] https://cccbdb.nist.gov/vibscale.asp.
[58] S. Poulindandurand, S. Perez, J.F. Revol, F. Brisse, Crystal-structure of poly (trimethylene terephthalate) by X-ray and electron-diffraction, Polymer 20 (4) (1979) 419–426.
[59] D. Galimberti, A. Milani, Crystal structure and vibrational spectra of poly (trimethylene terephthalate) from periodic density functional theory calculations, J. Phys. Chem. B 118 (7) (2014) 1954–1961.